

# Aging by near-extinctions in many-variable interacting populations

Thibaut Arnoux de Pirey and Guy Bunin

*Department of Physics, Technion-Israel Institute of Technology, Haifa 32000, Israel*

Models of many-species ecosystems, such as the Lotka-Volterra and replicator equations, suggest that these systems generically exhibit near-extinction processes, where population sizes go very close to zero for some time before rebounding, accompanied by a slowdown of the dynamics (aging). Here, we investigate the connection between near-extinction and aging by introducing an exactly solvable many-variable model, where the time derivative of each population size vanishes both at zero and some finite maximal size. We show that aging emerges generically when random interactions are taken between populations. Population sizes remain exponentially close (in time) to the absorbing values for extended periods of time, with rapid transitions between these two values. The mechanism for aging is different from the one at play in usual glassy systems: at long times, the system evolves in the vicinity of unstable fixed points rather than marginal ones.

Interactions between species in ecosystems may lead to large fluctuations in their population sizes. Theoretical models play a central role in understanding these fluctuations in nature and experiments, both for several species [1–4] and for many species [5]. The dynamics of populations that interact and reproduce are often modeled by coupled ordinary differential equations for population sizes  $\{x_i\}$ . They are non-negative variables,  $x_i \geq 0$ , and must remain so throughout the dynamics. The boundary values  $x_i(t) = 0$  represent extinct populations: if a population is extinct at some time  $t$ , it must remain so at all later times. Namely,  $x_i = 0$  is an absorbing value for  $x_i$ . These requirements are satisfied by a broad class of differential equations of the form [6]

$$\dot{x}_i = x_i g_i(\vec{x}). \quad (1)$$

Examples in this class include the Lotka-Volterra equations for which  $g_i(\vec{x}) = B_i - \sum_j A_{ij} x_j$ , with the matrix  $\mathbf{A}$  encoding the interactions between populations; resource-competition models [7]; and the replicator equations employed in evolution and game theory [6].

It is well-known that, depending on the shape of the functions  $g_i$ , few variable systems of the form (1) can exhibit different long-time behaviors such as stationarity, periodicity or chaos [6]. Remarkably, the existence of absorbing hyperplanes has also been shown to lead, in some cases, to robust heteroclinic cycles [8, 9]. A classical example is the three-species Lotka-Volterra system with rock-paper-scissors type interactions [10], where each species hinders the growth of the next. There, trajectories are attracted to a cycle connecting three unstable fixed points, each with a single surviving population, see Fig. 1(a). As time increases, they pass ever closer to these fixed points, resulting in slowdown of the dynamics, with exponentially increasing sojourn times in their vicinity and rapid transitions between them [10, 11].

In models characterized by a large number  $S$  of variables, recent works find that an analogous slowdown emerges generically for random interaction coefficients. It is known that aging (a situation in which the system

does not asymptotically settle to a fixed point but keeps exploring the phase space with a velocity that nevertheless decays with the elapsed time) can occur in many-variable Lotka-Volterra systems with random asymmetric interactions [12] and replicator equations with nearly antisymmetric random interactions [13]. Here, some populations experience ever longer periods near extinction ( $x_i \simeq 0$  and  $x_i$  closer to zero in successive near-extinction periods) before eventually returning to  $x_i = O(1)$ , see Fig. 1(b). Such dips and ‘blooms’ are documented in experiments and field data (e.g. [14, 15]), and are ecologically significant as they may lead to extinctions in actual finite populations. The properties of these dynamics have remained elusive, however. The analogy with low-dimensional examples such as in Fig. 1(a) is limited. For one, in the many-variable case, the system does not approach a limit-cycle (at least if the limit  $S \rightarrow \infty$  is taken before  $t \rightarrow \infty$ ). Secondly, large dynamical systems of the form (1) may possess many fixed points with different properties (e.g., the fraction of variables for which  $x_i = 0$  or their instability index), and linking the characteristics of fixed points to the dynamics remains an open problem.

In this work, we propose a high-dimensional model of the form (1) that provides insights into the connection between aging and absorbing values, by bypassing some of the difficulties inherent to the many-variable Lotka-Volterra and replicator equations. Fixed points of (1) satisfy either  $x_i = 0$  or  $g_i(\vec{x}) = 0$  for every  $i$ . Since the unique aging behavior of these systems is tied to the existence of absorbing values ( $x_i = 0$ ), we introduce a model with *two* absorbing values for each variable, which we refer to as the mirrored-extinction model. Specifically, we consider the evolution of  $S$  degrees of freedom  $\{x_i\}_{i=1,\dots,S}$ , with  $0 \leq x_i \leq 1$  for all  $i$ ,

$$\dot{x}_i(t) = x_i(t) \left[ 1 - x_i(t) \right] \sum_{j=1}^S \alpha_{ij} x_j(t), \quad (2)$$

where  $\alpha$  is a zero-mean Gaussian random matrix with

independent and identically distributed entries (referred to as asymmetric interactions). We take  $\mathbb{E}[\alpha_{ij}^2] = 1/S$  which sets the units of time. From an ecological perspective, the interactions in (2) affect the growth-rates of populations but not their maximal size, which might be limited by other factors, see for example [16, 17]. Equation (2) can be extended by adding a species-dependent growth rate  $g_i$  to the sum,  $\sum_j \alpha_{ij} x_j \rightarrow g_i + \sum_j \alpha_{ij} x_j$  (so that when a species is alone it undergoes simple logistic growth with a growth rate  $g_i$ , similarly to the Lotka-Volterra equations), and is solvable just as described below and with the same qualitative outcomes, see App. IV.

The resulting dynamical system has many fixed points where all degrees of freedom are at their absorbing values, either  $x_i = 0$  or  $x_i = 1$ , allowing us to focus on the effects of these absorbing boundaries. It displays aging, similarly to the Lotka-Volterra case, but with the  $x_i$  spending ever longer times close to either  $x_i = 0$  or 1 with rapid transitions between these two values, see Fig. 1(b). Importantly, the model in (2) is exactly solvable in high dimension, allowing us to obtain detailed information on the link between near-extinction processes and aging, beyond other models that also exhibit both phenomena [12, 13].

The mechanism for aging found here is drastically different from that at play in aging of usual spin-glasses following a quench, where the system's energy is reduced until it reaches an energy surface dominated by marginally-stable fixed points and spends its time there [18–20]. This includes Lotka-Volterra dynamics with *symmetric* interaction matrices  $\alpha_{ij}$  [21, 22], where  $\vec{g}(\vec{x})$  is the gradient of a potential, thus permitting a mapping to a spin-glass phase. This form of aging is known to disappear when asymmetry is introduced to the interaction coefficients [23, 24].

In contrast, here we show that aging happens in (2), as variables are driven close to their absorbing values: the probability  $P(x_i)$  at long times concentrates about  $\{0, 1\}$ , as shown below in (13). Near fixed points the dynamics slow down, as manifested in the autocorrelation  $C(t'+\tau, t')$  of  $x_i(t)$ , which as  $t'$  grows, relaxes more slowly with  $\tau$ , as shown below in (9). Similarly to the three-variable example of Fig. 1(a), typical systems go very close to fixed points which are therefore long-lived, see Fig. 1(b,c). This happens despite these fixed points being *unstable*, which we show by calculating the spectrum, Eq. (17), of the linearized dynamics around the fixed points approached at long times. This provides a mechanism for aging in the absence of an underlying energy function. We find that, in the long-time limit, the system moves between infinitely many unstable fixed points that all have the same finite fraction of unstable directions and the same stability spectrum. They are neither the most stable nor the most abundant fixed points.

*Dynamical mean field theory*—To analyze the many-variable dynamics (2), we use dynamical mean field the-

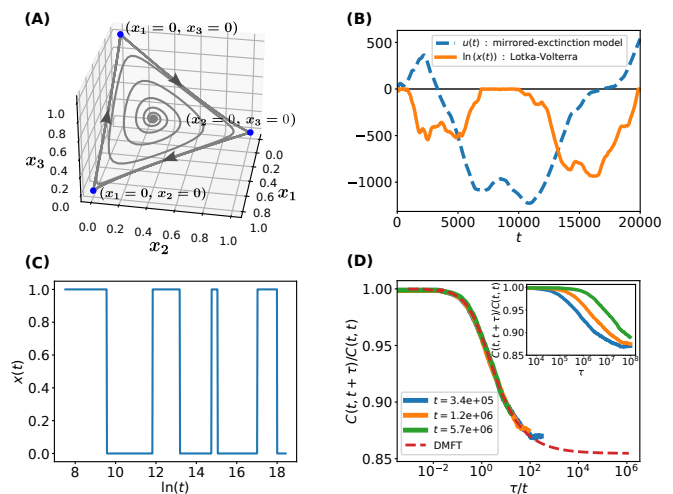


Figure 1. **Aging by passing near unstable fixed points.** (A) Heteroclinic cycle in the three-variable May-Leonard model. The dynamics slow down as the system goes ever closer to fixed points (dots), despite them being unstable. (B) Dynamics of example variables (out of  $S = 2 \cdot 10^4$ ), in the Lotka-Volterra system (solid line, plot of  $\ln x_i$ ) and the mirrored-extinction model (2), (dashed, plot of  $\ln[x_i/(1-x_i)]$ ). This illustrates the longer and deeper excursions near the absorbing values,  $x_i = 0$  for Lotka-Volterra and  $x_i \in \{0, 1\}$  for the mirrored-extinction case. (C) In log-time, the dynamics of any variable in (2) eventually follow a biased time-translation invariant two-state process. (D) Mean autocorrelation function  $C(t'+\tau, t')$  of  $x_i(t)$  as measured in a numerical simulation of (2) with  $2 \cdot 10^4$  degrees of freedom as a function of  $\tau/t'$ , showing a collapse for different waiting times  $t'$ , and agreement with the analytical master curve (dashed line). Inset: same curves, as a function of  $\tau$ . Parameters for Lotka-Volterra simulations in (A,B) are given in App. II.

ory (DMFT) [25, 26]. In the limit  $S \rightarrow \infty$  and for  $x_i$  sampled independently at the initial time, the dynamics of a single degree of freedom  $x(t)$  are exactly described by a stochastic differential equation

$$\dot{x}(t) = x(t)[1 - x(t)]\xi(t), \quad (3)$$

with  $\xi(t)$  a zero mean Gaussian process. This stems from the fact that the term  $\xi_i(t) \equiv \sum_j \alpha_{ij} x_j(t)$  appearing in (2) is the sum of many weakly correlated contributions. As is usual in DMFT, this expression for  $\xi_i(t)$  yields a self-consistent closure relation that reads  $C(t, t') \equiv \langle \xi(t)\xi(t') \rangle = \langle x(t)x(t') \rangle$ . Here the angular brackets  $\langle \cdot \rangle$  denote an average over the initial conditions  $x(0)$  and realizations of the noise  $\xi(t)$ . The derivation of (3) follows a standard procedure [12, 25–28] and is detailed in App. I. To analyze the dynamics, it is therefore very helpful to solve for the autocorrelation function  $C(t, t')$ .

To proceed, we introduce the transformation  $u(t) = \ln[x(t)/(1-x(t))]$  that sends the boundaries of the do-

main  $[0, 1]$  to  $(-\infty, +\infty)$  and for which (3) becomes

$$\dot{u}(t) = \xi(t), \quad (4)$$

with the closure relation

$$\langle \xi(t)\xi(t') \rangle = \langle f(u(t))f(u(t')) \rangle, \quad (5)$$

where

$$f(y) \equiv \frac{e^y}{1 + e^y}.$$

*Aging and the auto-correlation function*—We start by showing that the mean-square displacement of  $u(t)$  is ballistic. Denote the auto-correlation  $G(t, t') \equiv \langle u(t)u(t') \rangle$ , which by (4) is related to  $C(t, t')$  by  $C(t, t') = \partial_t \partial_{t'} G(t, t')$ . We take initial conditions such that  $u(0) = 0$ , or equivalently  $x(0) = 1/2$ ; the long-time behavior of the correlation function is insensitive to this choice. The closure equation in (5) can then be written as

$$\partial_t \partial_{t'} G(t, t') = \langle f(u(t))f(u(t')) \rangle. \quad (6)$$

$u(t), u(t')$  are jointly Gaussian with zero means, from which it follows that  $1/16 \leq \langle f(u(t))f(u(t')) \rangle \leq 1$ , see App. III. Therefore  $tt'/16 < G(t, t') < tt'$ , so  $\langle u(t)^2 \rangle = G(t, t) \sim t^2$ , corresponding to *ballistic* growth of  $u(t)$ . We show below that  $u(t)$  nonetheless repeatedly crosses the origin at arbitrarily long times.

The long-time expression for  $G(t, t')$  can be worked out from (6). Here we present a different but equivalent derivation, which makes explicit the aging properties of the model. Motivated by the ballistic growth of  $u(t)$ , we introduce  $z(t) \equiv u(t)/t$ , and we rescale time though  $s \equiv \ln(t)$ . The resulting dynamics read

$$z'(s) = -z(s) + \hat{\xi}(s), \quad (7)$$

together with the closure relation (from (5))

$$\langle \hat{\xi}(s)\hat{\xi}(s') \rangle = \langle f(e^s z(s))f(e^{s'} z(s')) \rangle.$$

Because  $z(s)$  is a Gaussian process with finite  $O(1)$  variance as  $s \rightarrow \infty$ , in the long-time limit this equation reads

$$\langle \hat{\xi}(s)\hat{\xi}(s') \rangle = \langle \Theta(z(s))\Theta(z(s')) \rangle. \quad (8)$$

Equations (7,8) map the original many-body dynamics of (2), in the long-time limit, to chaotic dynamics of random neural networks of the form discussed in [29]. As in [29], at large  $s$ , we expect the process in (7) to reach a time-translation invariant chaotic state characterized by

$$\langle \hat{\xi}(s)\hat{\xi}(s') \rangle \equiv \hat{C}(s - s').$$

In the original time scale  $t = e^s$ , this corresponds to autocorrelation of the form,

$$\lim_{t' \rightarrow \infty} C(t' + \tau, t') = \hat{C}(\ln(1 + \beta)), \quad (9)$$

at fixed  $\beta \equiv \tau/t'$ .  $C(t' + \tau, t')$  thus relaxes more slowly with  $\tau$  as  $t'$  grows, a hallmark of *aging*, here with correlation time growing linearly with the elapsed time. Accordingly, from (7), the  $z(s)$  autocorrelation function also admits a time-translation invariant form at large times

$$\langle z(s)z(s') \rangle \equiv \hat{\Delta}(s - s'),$$

which is related to  $G(t, t')$  through  $\lim_{t' \rightarrow \infty} G(t' + \tau, t')/t'(t' + \tau) = \hat{\Delta}(\ln(1 + \beta))$ . We now sketch the derivation of  $\hat{\Delta}$ . Following [29],  $\hat{\Delta}$  and  $\hat{C}$  are related by  $\hat{C}(s) = -\hat{\Delta}''(s) + \hat{\Delta}(s)$  which, together with (8), implies that  $\hat{\Delta}(s)$  satisfies an equation for the motion of a classical particle in a potential  $V$

$$\hat{\Delta}''(s) = -V'(\hat{\Delta}, \Delta_0), \quad (10)$$

where the potential depends parametrically on the initial condition  $\Delta_0 \equiv \hat{\Delta}(0)$  and reads,

$$V \equiv -\frac{\hat{\Delta}^2}{2} + \frac{\hat{\Delta}}{4} + \frac{\hat{\Delta}}{2\pi} \left( \sqrt{\frac{\Delta_0^2}{\hat{\Delta}^2} - 1} + \operatorname{arccot} \sqrt{\frac{\Delta_0^2}{\hat{\Delta}^2} - 1} \right).$$

The condition  $\hat{\Delta}(s) = \hat{\Delta}(-s)$  implies  $\hat{\Delta}'(0) = 0$  so that the  $\hat{\Delta}(s)$  trajectory has zero initial kinetic energy. The only physically relevant trajectory is therefore the one converging to the unstable fixed point  $\Delta^*$  with same potential energy as the initial condition and related to  $\Delta_0$  by  $V'(\Delta^*, \Delta_0) = 0$  and  $V(\Delta^*, \Delta_0) = V(\Delta_0, \Delta_0)$ . This gives  $\Delta_0 \simeq 0.476$  and  $\Delta^* \simeq 0.427$ .

The correlation  $C(t' + \tau, t') = \frac{1}{S} \sum_i x_i(t' + \tau)x_i(t')$ , obtained by running the dynamics (2), is thus expected by (9) to collapse when plotted against  $\tau/t'$ , as indeed seen in Fig. 1(d), and it matches the correlation function  $\hat{C}(s)$  obtained by numerically solving (10) with the appropriate initial conditions. Note that  $\Delta_0$  is linked to the long-time growth of  $\langle u(t)^2 \rangle$ , as  $G(t, t)/t^2 \xrightarrow{t \rightarrow \infty} \Delta_0$ . Additionally, the auto-correlation satisfies

$$\lim_{t' \rightarrow \infty} C(t', t') = \frac{1}{2} > \lim_{\tau \rightarrow \infty} \lim_{t' \rightarrow \infty} C(t' + \tau, t') = \Delta^*, \quad (11)$$

so that the system continues to evolve, as the correlation with the state at any time is later partially lost. Equation (10) implies a power law relaxation of  $C(t, t')$  in the aging regime to its plateau value  $\Delta^*$ ,

$$\lim_{t' \rightarrow \infty} C(t'(1 + \beta), t') - \Delta^* \sim_{\beta \rightarrow \infty} \beta^{-k},$$

with  $k = \sqrt{|V''(\Delta^*, \Delta_0)|} \simeq 0.492$ .

*Single variable dynamics*—The dynamics (2) pass very close to fixed points at long times. To see this, we calculate the probability distribution of  $x$  at time  $t$ ,  $P_t(x)$ , taken over many variables in (2), or equivalently over different realizations of (3). Using the fact that  $u(t)$  is Gaussian and that  $x(t) = f(u(t))$ , it reads

$$P_t(x) = \frac{[x(1-x)]^{-1}}{\sqrt{2\pi G(t,t)}} \exp \left[ -\frac{1}{2G(t,t)} \left( \ln \frac{x}{1-x} \right)^2 \right]. \quad (12)$$

In particular this implies,

$$\lim_{t \rightarrow \infty} P_t(x) = \frac{1}{2} [\delta(x) + \delta(x-1)]. \quad (13)$$

This shows that the system (2) *asymptotically approaches fixed points* of the dynamics, where all  $x_i \in \{0, 1\}$ . Furthermore, at large but finite times, the probability to find  $x(t)$  away from the boundaries of  $[0, 1]$  decays as  $1/t$ , with (12) giving

$$\text{Prob}[x(t) \in [\epsilon, 1-\epsilon]] \underset{t \rightarrow \infty}{\sim} \frac{1}{t} \sqrt{\frac{2}{\pi \Delta_0}} \ln \left( \frac{1-\epsilon}{\epsilon} \right). \quad (14)$$

for any fixed  $\epsilon \in [0, 1/2]$ . The probability is thus concentrated exponentially close in time to 0 and 1. Yet the system continues to evolve, see (11), so that none of these fixed points are stable: At long times the system transitions between unstable fixed points, spending ever longer times in their vicinity with fast transitions between them.

In the long-time limit, since  $x(s) = \Theta(z(s))$  for  $s \rightarrow \infty$ ,  $x(s)$  asymptotically approaches a time-translation invariant two-state process. This is illustrated in Fig. 1(c). Note that as  $\Delta^* > 0$  in (11), equation (13) is not the ergodic measure (in log-time) of a single variable  $x_i(t)$ . In App. V, we show that for a given degree of freedom the log-time ergodic measure is given by

$$P_{\bar{\xi}}(x) = (1-p)\delta(x) + p\delta(x-1), \quad (15)$$

with  $p = [1 + \text{Erf}(\bar{\xi}/\sqrt{2\chi})]/2$ , where  $\bar{\xi}$  is a zero mean Gaussian random variable with variance  $\langle \bar{\xi}^2 \rangle = \Delta^*$  and  $\chi = \int_0^\infty ds e^{-s} [\hat{C}(s) - \Delta^*]$ . So, in a given realization of (2), each variable has an ‘‘identity’’ expressed in the fraction of time (in log-time) it spends near 0 and 1.

*Stability of visited fixed points*—We found above that at long times the system approaches fixed points, but eventually leaves their vicinity, signaling that they are unstable. We now calculate their entire stability spectrum. The linearized dynamics close to a fixed point  $\mathbf{x}^*$  are  $\delta x_i = J_{ij} \delta x_j$  with a diagonal matrix  $J_{ij} = \delta_{ij} \lambda_i^*$ . The growth rates  $\lambda_i^*$ , positive when growing in the direction away from the boundaries, are given by

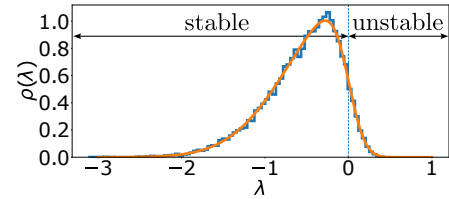


Figure 2. **Stability spectrum of the fixed points visited at long times.** The long-time dynamics evolve in the vicinity of unstable fixed points which all have the same stability spectrum. A finite fraction of the eigenvalues are positive, corresponding to unstable directions around these fixed points. The analytical prediction for the spectrum (17), is in excellent agreement with a simulation (blue) with  $S = 2 \cdot 10^4$  variables at  $t = 10^8$ .

$$\lambda_i^* = (1 - 2x_i^*) \left( \sum_j \alpha_{ij} x_j^* \right). \quad (16)$$

The stability spectrum of the visited fixed points is therefore equal, at long-times, to the empirical distribution in the many-variable dynamics (2) of  $\lambda_i(t) \equiv [1 - 2x_i(t)] \xi_i(t)$  for  $i = 1 \dots S$ . In the  $S \rightarrow \infty$  limit, the stability spectrum is thus equal to the distribution of  $\lambda(t) = [1 - 2x(t)] \xi(t)$  in the DMFT framework. It can also be shown that the  $\lambda_i(t)$  are independent and identically-distributed random variables, see App. VI, therefore the spectrum is self-averaging.

The joint distribution of  $\xi(t)$  and  $u(t)$  is Gaussian, with correlations  $\langle u(t)^2 \rangle = G(t,t)$ ,  $\langle \xi(t)^2 \rangle = C(t,t)$  and cross-correlation  $\langle u(t) \xi(t) \rangle$ . Changing variables from  $(u, \xi)$  to  $(u, \lambda)$  and integrating over  $u$ , we obtain an expression for the distribution of  $\lambda(t)$ , reproduced in App. VI. Taking its long-time limit, we find that the dynamics (2) transition between fixed points which all have the same stability spectrum

$$\rho(\lambda) = \frac{1}{\sqrt{\pi}} e^{-\lambda^2} \text{Erfc} \left( \frac{\lambda}{\kappa_\infty} \right), \quad (17)$$

with  $\kappa_\infty = \sqrt{1/(2\Delta_0) - 1} \simeq 0.224$ , see Fig. 2. This distribution has a *finite fraction of unstable directions*, given by

$$\int_0^\infty \rho(\lambda) d\lambda = \frac{\arctan(\kappa_\infty)}{\pi} \simeq 0.141.$$

Thus, the system approaches unstable fixed points. This can be compared with the statistics of the full distribution of fixed points of (2) with all  $x_i \in \{0, 1\}$ . There are  $2^S$  of them and the average number of those with  $\alpha S$  unstable directions is given by the binomial law,  $\langle \mathcal{N}_\alpha \rangle \sim \exp[Sg(\alpha)]$ , with  $g(\alpha) = -\alpha \ln \alpha - (1-\alpha) \ln(1-\alpha)$ .



Therefore, in typical fixed points half of the directions are unstable,  $\alpha = 1/2$ . The dynamics therefore selects in the long-time limit fixed points that are exponentially rare (compared to the typical ones) but that are not the most stable ones existing in the phase space, which are marginal ( $\alpha = 0$ ).

To conclude, we propose an exactly-solvable many-variable model for the dynamics of interacting populations with absorbing boundary values. Its dynamics slow down with a correlation time that grows as the age of the system, see (9). The system evolves in the vicinity of fixed points: In the long-time limit, all variables are found exponentially close in time to absorbing values, see (14). The time it takes for a variable to leave the vicinity of one absorbing value to visit the vicinity of the other is therefore proportional to the age of the system. This explains the scaling of the aging, (9). All these fixed points are unstable, as shown in (17), in contrast with marginal fixed points reached in usual glassy dynamics [18–20]. In the future, it would be interesting to understand how this scenario is adapted to other many-variable interacting population dynamics, such as the Lotka-Volterra model, where fixed points have degrees of freedom that are not at absorbing values. Fingerprints of these phenomena might be observed, as an increase in correlation time combined with population blooms, in experiments that follow interacting species starting from similar population sizes.

*Acknowledgments*—G. B. was supported by the Israel Science Foundation (ISF) Grant No. 773/18.

- 
- [1] Elisa Benincà, Bill Ballantine, Stephen P Ellner, and Jef Huisman. Species fluctuations sustained by a cyclic succession at the edge of chaos. *Proceedings of the National Academy of Sciences*, 112(20):6389–6394, 2015.
- [2] Gregor F Fussmann, Stephen P Ellner, Kyle W Shertzer, and Nelson G Hairston Jr. Crossing the hopf bifurcation in a live predator-prey system. *Science*, 290(5495):1358–1360, 2000.
- [3] G. F. Gause. Experimental analysis of vito volterra’s mathematical theory of the struggle for existence. *Science*, 79(2036):16–17, 1934.
- [4] Ophelia S Venturelli, Alex V Carr, Garth Fisher, Ryan H Hsu, Rebecca Lau, Benjamin P Bowen, Susan Hromada, Trent Northen, and Adam P Arkin. Deciphering microbial interactions in synthetic human gut microbiome communities. *Molecular systems biology*, 14(6):e8157, 2018.
- [5] Jiliang Hu, Daniel R Amor, Matthieu Barbier, Guy Bunin, and Jeff Gore. Emergent phases of ecological diversity and dynamics mapped in microcosms. *Science*, 378(6615):85–89, 2022.
- [6] Josef Hofbauer and Karl Sigmund. *Evolutionary games and population dynamics*. Cambridge university press, 1998.
- [7] Robert Mac Arthur. Species packing, and zhat competition minimizes. *Proceedings of the National Academy of Sciences*, 64(4):1369–1371, December 1969.
- [8] M Krupa. Robust heteroclinic cycles. page 48.
- [9] Josef Hofbauer. Heteroclinic cycles in ecological differential equations. *Mathematical Institute, Slovak Academy of Sciences*, 1994.
- [10] Robert M. May and Warren J. Leonard. Nonlinear Aspects of Competition Between Three Species. *SIAM Journal on Applied Mathematics*, 29(2):243–253, September 1975.
- [11] Andrea Gaunersdorfer. Time Averages for Heteroclinic Attractors. *SIAM Journal on Applied Mathematics*, 52(5):1476–1489, October 1992.
- [12] F Roy, G Biroli, G Bunin, and C Cammarota. Numerical implementation of dynamical mean field theory for disordered systems: application to the Lotka-Volterra model of ecosystems. *Journal of Physics A: Mathematical and Theoretical*, 52(48):484001, November 2019.
- [13] Michael T. Pearce, Atish Agarwala, and Daniel S. Fisher. Stabilization of extensive fine-scale diversity by ecologically driven spatiotemporal chaos. *Proceedings of the National Academy of Sciences*, 117(25):14572–14583, June 2020.
- [14] Antonio M. Martin-Platero, Brian Cleary, Kathryn Kauffman, Sarah P. Preheim, Dennis J. McGillicuddy, Eric J. Alm, and Martin F. Polz. High resolution time series reveals cohesive but short-lived communities in coastal plankton. *Nature Communications*, 9(1):266, January 2018. Number: 1 Publisher: Nature Publishing Group.
- [15] J. Cesar Ignacio-Espinoza, Nathan A. Ahlgren, and Jed A. Fuhrman. Long-term stability and Red Queen-like strain dynamics in marine viruses. *Nature Microbiology*, 5(2):265–271, February 2020. Number: 2 Publisher: Nature Publishing Group.
- [16] Christoph Ratzke and Jeff Gore. Modifying and reacting to the environmental pH can drive bacterial interactions. *PLOS Biology*, 16(3):e2004248, March 2018.
- [17] Christoph Ratzke, Julien Barrere, and Jeff Gore. Strength of species interactions determines biodiversity and stability in microbial communities. *Nature Ecology & Evolution*, 4(3):376–383, March 2020.
- [18] L. F. Cugliandolo and J. Kurchan. Analytical solution of the off-equilibrium dynamics of a long-range spin-glass model. *Physical Review Letters*, 71(1):173–176, July 1993.
- [19] Jorge Kurchan and Laurent Laloux. Phase space geometry and slow dynamics. *Journal of Physics A: Mathematical and General*, 29(9):1929–1948, May 1996.
- [20] Alessandro Manacorda and Francesco Zamponi. Gradient descent dynamics and the jamming transition in infinite dimensions. *arXiv:2201.01161 [cond-mat]*, January 2022. arXiv: 2201.01161.
- [21] Ada Altieri, Felix Roy, Chiara Cammarota, and Giulio Biroli. Properties of Equilibria and Glassy Phases of the Random Lotka-Volterra Model with Demographic Noise. *Physical Review Letters*, 126(25):258301, June 2021.
- [22] Giulio Biroli, Guy Bunin, and Chiara Cammarota. Marginally stable equilibria in critical ecosystems. *New Journal of Physics*, 20(8):083051, August 2018.
- [23] Leticia F. Cugliandolo, Jorge Kurchan, Pierre Le Doussal, and Luca Peliti. Glassy behaviour in disordered systems with nonrelaxational dynamics. *Physical Review Letters*, 78(2):350–353, January 1997.
- [24] A. Crisanti and H. Sompolinsky. Dynamics of spin

- systems with randomly asymmetric bonds: Langevin dynamics and a spherical model. *Physical Review A*, 36(10):4922–4939, November 1987.
- [25] Marc Mezard, Giorgio Parisi, and Miguel Angel Virasoro. *Spin Glass Theory And Beyond: An Introduction To The Replica Method And Its Applications*. World Scientific Publishing Company, November 1987.
- [26] H. Sompolinsky and Annette Zippelius. Relaxational dynamics of the Edwards-Anderson model and the mean-field theory of spin-glasses. *Physical Review B*, 25(11):6860–6875, June 1982.
- [27] Chen Liu, Giulio Biroli, David R. Reichman, and Grzegorz Szamel. Dynamics of liquids in the large-dimensional limit. *Physical Review E*, 104(5):054606, November 2021.
- [28] Elisabeth Agoritsas, Giulio Biroli, Pierfrancesco Urbani, and Francesco Zamponi. Out-of-equilibrium dynamical mean-field equations for the perceptron model. *Journal of Physics A: Mathematical and Theoretical*, 51(8):085002, February 2018.
- [29] H. Sompolinsky, A. Crisanti, and H. J. Sommers. Chaos in Random Neural Networks. *Physical Review Letters*, 61(3):259–262, July 1988.
- [30] Marc Mézard. The space of interactions in neural networks: Gardner’s computation with the cavity method. *Journal of Physics A: Mathematical and General*, 22(12):2181, 1989.
- [31] Elisabeth Agoritsas, Thibaud Maimbourg, and Francesco Zamponi. Out-of-equilibrium dynamical equations of infinite-dimensional particle systems i. the isotropic case. *Journal of Physics A: Mathematical and Theoretical*, 52(14):144002, 2019.
- [32] Guy Bunin. Ecological communities with Lotka-Volterra dynamics. *Physical Review E*, 95(4):042414, April 2017.
- [33] Florent Krzakala, Federico Ricci-Tersenghi, Lenka Zdeborova, Riccardo Zecchina, Eric W. Tramel, and Leticia F. Cugliandolo. *Statistical Physics, Optimization, Inference, and Message-Passing Algorithms: Lecture Notes of the Les Houches School of Physics: Special Issue, October 2013*. Oxford University Press, December 2015.

Supplemental material for “Aging by near-extinctions in many-variable interacting populations”

I. DYNAMICAL MEAN FIELD THEORY

We derive (3) of the main text using the cavity method, used in many fields such as mean-field spin glasses [25], neural networks [30], interacting particle systems in large dimension [27, 31] and many-variable population dynamics [12, 32]. In the many-body dynamics (2) of the main text, each degree of freedom  $x_i$  is driven by a ‘field’  $\xi_i(t)$

$$\xi_i(t) \equiv \sum_j \alpha_{ij} x_j(t),$$

which is expressed as a sum over all the contributions coming from the other many degrees of freedom it interacts with. Since for any  $i$  the different interaction coefficients  $\alpha_{ij}$  are *i.i.d.* random numbers it is natural to expect that  $\xi_i(t)$  converges to a Gaussian process in the large system-size limit  $S \rightarrow \infty$ . In the cavity method, this is shown by investigating how the dynamics of a single degree of freedom, say here  $x_0(t)$ , perturbs that of the ones it is coupled to and by expressing  $\xi_0(t)$  only in terms of  $x_i^{(0)}(t)$  for  $i > 0$ , the evolution of the other degrees of freedom in an identical system where all couplings to  $x_0(t)$  would be set to zero. This eventually allows to apply the central limit theorem and to cast the evolution of  $x_i(t)$  in the form of a stochastic differential equation, see (3) of the main text. To proceed, we start by considering the dynamics of  $S$  degrees of freedom subjected to a perturbation field  $h_i(t)$  acting as

$$\dot{x}_i = x_i(1 - x_i) \left( \sum_{j=1}^S \alpha_{ij} x_j + h_i \right).$$

For now the field  $h_i(t)$  is arbitrary but will later represent the perturbation induced by the coupling to an additional degree of freedom. The linear response function

$$R_{ij}(t, s) = \left. \frac{\delta x_i(t)}{\delta h_j(s)} \right|_{\mathbf{h}=0},$$

obeys

$$\partial_t R_{ij}(t, s) = (1 - 2x_i) \left( \sum_{j \neq i} \alpha_{ij} x_j \right) R_{ij}(t, s) + x_i(1 - x_i) \left( \delta_{ij} \delta(t - s) + \sum_{k \neq i, j} \alpha_{ik} R_{kj}(t, s) + \alpha_{ij} R_{jj}(t, s) \right).$$

From the above equation it follows that  $R_{ii}(t, t) = x_i(t) [1 - x_i(t)]$  and  $R_{ij}(t, t) = 0$  for  $j \neq i$ , from which one can deduce the scalings  $R_{ii}(t, s) = O(1)$  and  $R_{ij}(t, s) = \alpha_{ij} \hat{R}_{ij}(t, s)$  with  $\hat{R}_{ij}(t, s) = O(1)$  for  $i \neq j$ . We can now proceed with the cavity method, by considering a system comprised of  $S + 1$  degrees of freedom from which we arbitrarily single out one, labeled  $x_0$ . In the following the indices  $i, j$  run from 1 to  $S$ . The dynamics of  $x_0$  read

$$\dot{x}_0 = x_0(1 - x_0) \sum_i \alpha_{0i} x_i, \tag{1}$$

and that of the  $x_i$  read

$$\dot{x}_i = x_i(1 - x_i) \left( \sum_{j \neq i} \alpha_{ij} x_j + \alpha_{i0} x_0 \right). \tag{2}$$

Therefore a given trajectory of  $x_0$  acts on the  $x_i$  as the previously introduced perturbing field  $\mathbf{h}$ , when setting  $h_i = \alpha_{i0} x_0$ . For a given initial condition  $x_i(0)$  and a given trajectory  $x_0(t)$  we decompose the motion of the  $x_i(t)$  as

$x_i(t) = x_i^{(0)}(t) + \delta x_i[x_0](t)$  where  $x_i^{(0)}(t)$  is the solution of (2) when all the couplings  $\alpha_{i0}$  for  $i = 1 \dots S$  are set to zero and  $\delta x_i[x_0]$  accounts for the correction of the solution due to the dynamics of  $x_0$ . It follows from (1) that describing the dynamics of  $x_0(t)$  to  $O(1)$  in  $S$  only requires to know  $\delta x_i[x_0](t)$  up to order  $O(1/\sqrt{S})$ . We can therefore find  $\delta x_i$  within linear-response, which up to  $O(1/S)$  corrections can be written as

$$\delta x_i[x_0](t) = \int_0^t ds \left( R_{ii}(t, s) \alpha_{i0} + \sum_{j \neq i} R_{ij}(t, s) \alpha_{j0} \right) x_0(s).$$

Therefore we have to order  $O(1)$ ,

$$\dot{x}_0 = x_0(1 - x_0) \left[ \sum_i \alpha_{0i} x_i^{(0)} + \int_0^t ds \sum_i \alpha_{0i} \left( R_{ii}(t, s) \alpha_{i0} + \sum_{j \neq i} R_{ij}(t, s) \alpha_{j0} \right) x_0(s) \right].$$

Because the interaction matrix is fully asymmetric,  $\mathbb{E}[\alpha_{0j} \alpha_{i0}] = 0$ , the contribution from the linear response term,  $\int_0^t ds \dots$ , scales as  $O(1/\sqrt{S})$  and can be neglected. The dynamics of  $x_0$  hence read, up to  $O(1/\sqrt{S})$  corrections,

$$\dot{x}_0 = x_0(1 - x_0) \sum_i \alpha_{0i} x_i^{(0)}.$$

We now assume that  $x_i^{(0)}$  and  $x_j^{(0)}$  (or equivalently  $x_i$  and  $x_j$ ) are weakly correlated processes for  $i \neq j$  meaning that for any functional  $F[x(t)]$  we have

$$\mathbb{E} \left[ \left( F[x_i^{(0)}(t)] - \mathbb{E}[F[x^{(0)}(t)]] \right) \left( F[x_j^{(0)}(t)] - \mathbb{E}[F[x^{(0)}(t)]] \right) \right] \xrightarrow{S \rightarrow \infty} 0, \quad (3)$$

where we have stressed the fact that all variables are statistically identical. Such an assumption, which can be verified self-consistently (see below), is standard in DMFT [33]. It implies a law of large numbers, namely that for any functional  $F[x(t)]$

$$\frac{1}{S} \sum_i F[x_i^{(0)}(t)] \xrightarrow{S \rightarrow \infty} \mathbb{E}[F[x^{(0)}(t)]],$$

in agreement with the self-averaging property of the auto-correlation function shown numerically in Fig. 1(D) of the main text. In the large  $S$  limit,  $\xi_i \equiv \sum_i \alpha_{0i} x_i^0$  thus converges to a Gaussian process with zero mean and variance

$$\mathbb{E}[\xi_i(t) \xi_i(t')] = \mathbb{E}[x^{(0)}(t) x^{(0)}(t')] = \mathbb{E}[x_0(t) x_0(t')]$$

where we used that, up to order  $O(1)$ ,  $x_i^{(0)}$  and  $x_i$  and  $x_0$  are statistically identical. This proves (3) of the main text. To see that the weak correlation assumption, (3), is self-consistent within DMFT, we note that the  $O(1)$  dynamics of two degrees of freedom  $x_0$  and  $x_1$  read (as the direct interactions between them are only  $O(S^{-1/2})$ )

$$\dot{x}_0 = x_0(1 - x_0) \sum_{i>1} \alpha_{0i} x_i^{(0,1)},$$

and

$$\dot{x}_1 = x_1(1 - x_1) \sum_{i>1} \alpha_{1i} x_i^{(0,1)},$$

where  $x_i^{(0,1)}$  refers to the solution of the many-body dynamics in the absence of both  $x_0$  and  $x_1$ . Upon assuming that (3) holds, the moment generating function of  $\xi_0 = \sum_{i>1} \alpha_{0i} x_i^{(0,1)}$  and  $\xi_1 = \sum_{i>1} \alpha_{1i} x_i^{(0,1)}$  can be worked out showing that they are independent and identically distributed Gaussian processes. To leading order, the statistical independence of  $x_0$  and  $x_1$  then follows, in agreement with (3). This also implies that the exponential growth rates  $\lambda_i(t) \equiv [1 - 2x_i(t)] \xi_i(t)$  in (16) of the main text at the dynamically visited fixed points behave, to leading order, as independent and identically distributed random variables in the limit of a large number of degrees of freedom  $S \rightarrow \infty$ .



## II. LOTKA-VOLTERRA SIMULATIONS

In Fig. 1(A) of the main text, the interaction matrix  $\mathbf{A}$  is cyclic with  $A_{ii} = 1$ ,  $A_{i,i+1} = 0.3$ ,  $A_{i,i-1} = 2$ , and all  $B_i = 1$ . In Fig. 1(B),  $S = 2 \cdot 10^4$ . The parameters of the Lotka-Volterra dynamics are  $B_i = 1$  and an interaction matrix  $\mathbf{A}$  defined by  $A_{ii} = 1$  and  $A_{ij}$  for  $i \neq j$  Gaussian variables with mean  $\mathbb{E}[A_{ij}] = 10/S$  and variance  $\mathbb{E}[A_{ij}A_{kl}] = 2\delta_{ik}\delta_{jl}/S$ .

## III. PROOF OF BOUNDS ON $\langle f(u(t)) f(u(t')) \rangle$

Here we derive the bounds

$$1/16 \leq \langle f(u(t)) f(u(t')) \rangle \leq 1,$$

stated in the main text, below Eq. (6) there. Indeed, we have first

$$0 < \frac{e^u}{1+e^u} < 1 \Rightarrow \langle f(u(t)) f(u(t')) \rangle < 1.$$

To obtain the lower bound, observe that  $u(t)$  and  $u(t')$  are jointly Gaussian with correlation matrix

$$M(t, t') = \begin{pmatrix} G(t, t) & G(t, t') \\ G(t, t') & G(t', t') \end{pmatrix}.$$

Therefore

$$\begin{aligned} \langle f(u(t)) f(u(t')) \rangle &> \int_0^{+\infty} \int_0^{+\infty} \frac{du_1}{\sqrt{2\pi}} \frac{du_2}{\sqrt{2\pi}} \frac{\exp(-\frac{1}{2} u^T \cdot M^{-1}(t, t') \cdot u)}{\sqrt{\det M(t, t')}} f(u_1) f(u_2) \\ &> \frac{1}{4} \int_0^{+\infty} \int_0^{+\infty} \frac{du_1}{\sqrt{2\pi}} \frac{du_2}{\sqrt{2\pi}} \frac{\exp(-\frac{1}{2} u^T \cdot M^{-1}(t, t') \cdot u)}{\sqrt{\det M(t, t')}} = \frac{1}{16} \left( 1 + \frac{2}{\pi} \operatorname{arccot} \sqrt{\frac{G(t, t)G(t', t')}{G(t, t')^2} - 1} \right) > \frac{1}{16}. \end{aligned}$$

This completes the proof.

## IV. ADDING A NON-ZERO GROWTH RATE

The phenomenology presented in the main text can be extended to the case where a non-zero bare growth rate is taken into account, *i.e.* for the system of equations

$$\dot{x}_i = x_i(1 - x_i) \left( g_i + \sum_{j=1}^S \alpha_{ij} x_j \right), \quad (1)$$

for  $i = 1 \dots S$  where  $g_i$  are *i.i.d* species-dependent growth rates sampled from the distribution  $P(g)$  and  $\alpha$  the interaction matrix which is assumed to be Gaussian with zero mean and variance  $\mathbb{E}[\alpha_{ij}\alpha_{mn}] = \delta_{im}\delta_{jn}/S$ . The analysis follows the one presented in the main text for  $g_i = 0$ . The derivation of the DMFT equations presented in App. I applies and in the limit  $S \rightarrow \infty$  the effective stochastic process reads

$$\dot{x} = x(1 - x)(g + \xi(t)),$$

with  $g$  a random variable sampled from  $P(g)$  which extends (3) of the main text and where  $\xi(t)$  is a zero-mean Gaussian noise with variance  $\langle \xi(t)\xi(t') \rangle = \langle x(t)x(t') \rangle$  where the average in the right-hand side is now taken over the realisations of both the noise and the growth rate. If the distribution  $P(g)$  has a non-zero support on  $[0, +\infty[$ , then the bounds of App. III can be adapted and read

$$\frac{1}{16} \int_0^{+\infty} dg P(g) \leq \langle \xi(t)\xi(t') \rangle \leq 1.$$

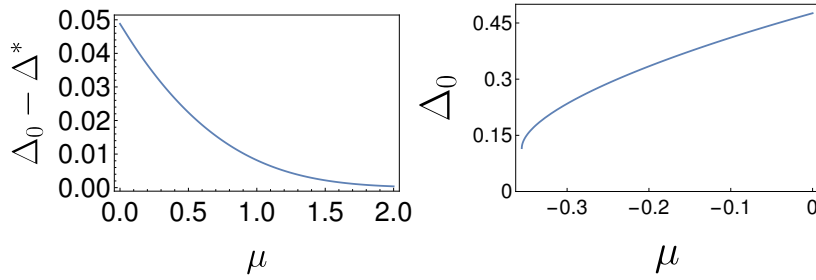


Figure 3. **Amplitude of the dynamical fluctuations of  $\tilde{z}(s)$  as a function of the bare growth rate  $\mu$  when all  $g_i = \mu$ .** Left: As  $\mu \geq 0$  increases, the amplitude of the temporal fluctuations  $\Delta_0 - \Delta^*$  decays continuously to zero at large  $\mu$ . Right: For  $\mu \leq \mu_c \approx -0.35$  the system collapses to the trivial fixed point with all  $x_i = 0$ . Shown is the equal-time correlation function  $\Delta_0$  as a function of  $\mu$  for  $\mu \leq 0$ .

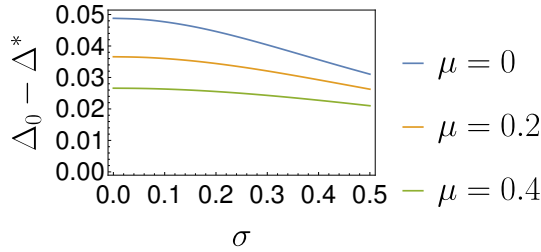


Figure 4. **Amplitude of the dynamical fluctuations of  $\tilde{z}(s)$  as a function of the standard deviation  $\sigma$  of the distribution  $P(g)$  for different values of  $\mu$ .** The amplitude of the fluctuations  $\Delta_0 - \Delta^*$  is a decreasing function of  $\sigma$ .

Accordingly, by defining  $s = \ln t$  and  $z = \ln [x/(1-x)]/t$ , (7) of the main text becomes

$$z'(s) = -z(s) + g + \hat{\xi}(s), \quad (2)$$

with (8) holding in the long-time limit. We introduce  $\tilde{z}(s) = z(s) - g$  and denote its autocorrelation function  $\langle \tilde{z}(s)\tilde{z}(s') \rangle \equiv \tilde{\Delta}(s-s')$  which is related to that of the process  $z(s)$  by  $\langle \tilde{z}(s)\tilde{z}(s') \rangle \equiv \langle z(s)z(s') \rangle - \langle g^2 \rangle$ . The equation for the evolution of  $\tilde{\Delta}''(s)$  then follows from

$$\tilde{\Delta}''(s) = -V'(\tilde{\Delta}, \Delta_0),$$

where  $\Delta_0 = \tilde{\Delta}(0)$  and the effective potential  $V(\tilde{\Delta}, \Delta_0)$  reads

$$V \equiv -\frac{\tilde{\Delta}^2}{2} + \frac{\tilde{\Delta}}{4} \left( 1 + \int_{-\infty}^{+\infty} dg P(g) \operatorname{Erf} \left( \frac{g}{\sqrt{2\Delta_0}} \right) \right) + \int_{-\infty}^{+\infty} dg P(g) \int_0^{+\infty} \frac{dx}{2\sqrt{2\pi\Delta_0}} e^{-\frac{(x-g)^2}{2\Delta_0}} \int_0^{\tilde{\Delta}} d\Delta \operatorname{Erf} \left( \frac{g(\Delta_0 - \Delta) + x\Delta}{\sqrt{2\Delta_0(\Delta_0^2 - \Delta^2)}} \right).$$

Following the discussion of the main text, we find  $\Delta_0$  and  $\Delta^* = \lim_{s \rightarrow \infty} \tilde{\Delta}(s)$  by requiring that  $V(\Delta^*, \Delta_0) = V(\Delta_0, \Delta_0)$  together with  $V'(\Delta^*, \Delta_0) = 0$ . We first consider the case  $P(g) = \delta(g - \mu)$ , corresponding to an identical bare growth rate for all the species. If  $\mu \geq 0$ , the behavior is similar to the  $g = 0$  case studied at depth in the main text. The noise splits into two independent contributions: one static and one with time-translation invariant statistics in log-time. The amplitude of the temporal fluctuations of the process  $\tilde{z}(s)$  varies continuously with the bare growth rate  $\mu$  and decays to zero at large  $\mu$ , see Fig. 3. All the degrees of freedom in (2) are indeed expected to reach the limit  $x_i(t) \xrightarrow{t \rightarrow \infty} 1$  and dynamical fluctuations to be suppressed in this limit. If  $\mu \leq 0$ , numerical solutions of the equations for  $\Delta_0$  and  $\Delta^*$  suggest that there exists a finite value  $\mu_c \leq 0$  such that for strong enough negative rate  $\mu \leq \mu_c$ , we have  $\Delta_0 = \Delta^* = 0$  corresponding to the trivial fixed point where all species are extinct,  $x_i = 0$ , see Fig. 3. We also investigated the case where there is heterogeneity in the growth rates by taking  $P(g)$  Gaussian with mean  $\mu$  and standard deviation  $\sigma$ . The results remain qualitatively the same, with the amplitude of the fluctuations decreasing with  $\sigma$ , see Fig. 4.

The derivation can be extended to account for the existence of species-dependent growth rates  $g_i$ , in the case where the  $g_{i=1\dots S}$  are identically distributed and sampled independently from each other and from the elements of the interaction matrix  $\alpha$  from a distribution  $P(g)$ .

## V. ERGODIC MEASURE FOR $x(s)$

We recall (7) of the main text

$$z'(s) = -z(s) + \hat{\xi}(s), \quad (1)$$

and decompose the noise  $\hat{\xi}(s)$  as

$$\hat{\xi}(s) = \bar{\xi} + \delta\xi(s)$$

with  $\bar{\xi}$  a Gaussian random variable with zero mean and variance  $\langle \bar{\xi}^2 \rangle = \Delta^*$  and  $\delta\xi(s)$  an independent Gaussian process with zero mean and covariance

$$\langle \delta\xi(s)\delta\xi(s') \rangle = \hat{C}(s, s') - \Delta^*.$$

In the long-time limit, the solution to (1) reads

$$z(s) = \bar{\xi} + e^{-s} \int_0^s ds' e^{-s'} \delta\xi(s'),$$

so that at large  $s$ , and fixed  $\bar{\xi}$ ,  $z(s)$  is a Gaussian variable with mean  $\bar{\xi}$  and variance

$$\langle (z(s) - \bar{\xi})^2 \rangle \xrightarrow{s \rightarrow \infty} \int du e^{-u} [\hat{C}(u) - \Delta^*].$$

Equation (15) of the main text then follows,

$$P_{\bar{\xi}}(x) = (1-p)\delta(x) + p\delta(x-1), \quad (2)$$

with  $p = [1 + \text{Erf}(\bar{\xi}/\sqrt{2\chi})]/2$ , where  $\bar{\xi}$  is a zero mean Gaussian random variable with variance  $\langle \bar{\xi}^2 \rangle = \Delta^*$  and  $\chi = \int_0^\infty ds e^{-s} [\hat{C}(s) - \Delta^*]$ . While each variable switches between 0 and 1 an infinite amount of time, the probability distribution of  $p$  (the fraction, in log-time, spent at  $x=1$ ) diverges at 0 (and accordingly at 1) as,

$$P(p) \underset{p \rightarrow 0}{\sim} \left( p\sqrt{-\ln p} \right)^{-1 + \frac{\chi}{\sqrt{\Delta^*}}},$$

with  $\chi/\sqrt{\Delta^*} \simeq 0.92$ . Namely, some degrees of freedom are strongly biased towards one of the boundaries.

## VI. STABILITY SPECTRUM

As stated in the main text, the joint distribution of  $\xi(t)$  and  $u(t)$  is Gaussian,

$$P_t(u, \xi) = \frac{1}{2\pi\sqrt{\det \mathbf{H}}} \exp \left[ -\frac{1}{2} (u, \xi) \cdot \mathbf{H}^{-1} \cdot (u, \xi) \right], \quad (1)$$

with the matrix  $\mathbf{H}$  given by

$$\mathbf{H} = \begin{pmatrix} G(t, t) & \langle u(t)\xi(t) \rangle \\ \langle u(t)\xi(t) \rangle & C(t, t) \end{pmatrix}.$$

Using this equation, changing variables to  $(u, \lambda)$  and integrating over  $u$ , the probability distribution of  $\lambda(t)$  is found to be

$$\begin{aligned} \rho_t(\lambda) = & \frac{\sqrt{1+\kappa^2}}{\kappa\sqrt{\pi C(t, t)}} \int_0^{+\infty} \frac{du}{\sqrt{\pi}} \exp \left[ -\frac{1+\kappa(t)^2}{2\kappa(t)^2} u^2 - \frac{1+\kappa(t)^2}{2\kappa(t)^2} \frac{\lambda^2}{C(t, t)} \left( \frac{1 - e^{\sqrt{G(t, t)u}}}{1 + e^{\sqrt{G(t, t)u}}} \right)^2 \right. \\ & \left. + \frac{\sqrt{1+\kappa(t)^2}}{\kappa(t)^2 \sqrt{C(t, t)}} u \lambda \left( \frac{1 - e^{\sqrt{G(t, t)u}}}{1 + e^{\sqrt{G(t, t)u}}} \right)^2 \right] \\ & \times \left| \frac{1 - e^{\sqrt{G(t, t)u}}}{1 + e^{\sqrt{G(t, t)u}}} \right|, \end{aligned} \quad (2)$$

with

$$\kappa(t) = \sqrt{\frac{C(t,t)G(t,t)}{\langle u(t)\xi(t) \rangle^2} - 1}.$$

At long times,

$$\kappa(t) \rightarrow \kappa_\infty = \lim_{t \rightarrow \infty} \sqrt{\frac{\Delta_0}{2 \left( \int_0^1 C(ts, t) ds \right)^2} - 1} = \sqrt{\frac{1}{2\Delta_0} - 1} \simeq 0.224.$$

where the last equality was obtained by noting that

$$\lim_{t \rightarrow \infty} \int_0^1 C(ts, t) ds = \int_0^{+\infty} ds e^{-s} \hat{C}(s) = \int_0^{+\infty} ds e^{-s} [-\hat{\Delta}''(s) + \hat{\Delta}(s)] = - \int_0^{+\infty} ds \frac{d}{ds} \left\{ e^{-s} [\hat{\Delta}'(s) + \hat{\Delta}(s)] \right\} = \Delta_0.$$

At  $t \rightarrow \infty$ , equation (2) reduces to (17) of the main text.